Featured in Physics

In Situ Measurement of Electron Energy Evolution in a Laser-Plasma Accelerator

S. Bohlen,[1,2,*] T. Brümmer,[1] F. Grüner,[2] C. A. Lindstrøm,[1] M. Meisel,[1,2] T. Staufer,[2] M. J. V. Streeter,[1,3] M. C. Veale,[4] J. C. Wood,[1] R. D'Arcy,[1] K. Põder,[1] and J. Osterhoff[1]

[1]*Deutsches Elektronen-Synchrotron DESY, Notkestraße 85, 22607 Hamburg, Germany*

[2]*Universität Hamburg and Center for Free-Electron Laser Science, Luruper Chaussee 149, 22761 Hamburg, Germany*

[3]*Centre for Plasma Physics, School of Mathematics and Physics, Queen's University Belfast, BT7 1NN, Belfast, United Kingdom*

[4]*UKRI STFC, Rutherford Appleton Laboratory, Didcot, OX11 0QX, United Kingdom*

(Received 20 October 2021; revised 22 July 2022; accepted 12 October 2022; published 6 December 2022)

We report on a novel, noninvasive method applying Thomson scattering to measure the evolution of the electron beam energy inside a laser-plasma accelerator with high spatial resolution. The determination of the local electron energy enabled the *in-situ* detection of the acting acceleration fields without altering the final beam state. In this Letter we demonstrate that the accelerating fields evolve from (265 ± 119) GV/m to (9 ± 4) GV/m in a plasma density ramp. The presented data show excellent agreement with particle-in-cell simulations. This method provides new possibilities for detecting the dynamics of plasma-based accelerators and their optimization.

DOI: 10.1103/PhysRevLett.129.244801

In laser-plasma acceleration (LPA) [1] electric fields of order $\mathcal{O}(100\ \mathrm{GV/m})$ can be generated to accelerate electron bunches to highly relativistic energies over short distances, outperforming radio-frequency (RF) devices by orders of magnitude. After the first demonstration of quasi-mono-energetic beams in 2004 [2–4], the energy frontier of LPA has been pushed continuously [5–7], now reaching more than 8 GeV [8], within range of state-of-the-art RF free-electron lasers (FELs). While first gain in a plasma-based FEL was achieved recently [9], the quality of bunches from LPA needs further improvement to fully compete with conventional accelerators. Measuring the beam properties during acceleration is a crucial step toward understanding and controlling the plasma-acceleration process. Currently particle-in-cell (PIC) simulations are the primary tool for determining the evolution of electron-beam parameters as state-of-the-art diagnostic methods are limited to observing the final state [10]. Noninvasive methods, capable of determining electron parameters during evolution in plasma, such as streaked betatron radiation, are highly desirable and have been proposed [11] but have yet to be experimentally demonstrated. An alternative approach would be to change the acceleration length, which is possible [12–15] but invasive and can be complex.

In this Letter, we report on the application of Thomson scattering [16] as a noninvasive technique for determining the energy evolution of an electron bunch during acceleration in a plasma wake. The measurements show excellent agreement with PIC simulations and had no discernible effect on the final state of the electron beam. This method enables *in situ* characterization of the development of electron-bunch parameters with arbitrary wake drivers and injection mechanisms.

Thomson scattering is the elastic scattering of a photon and an electron ignoring the recoil effect of the electron, where the photon gains energy from a relativistic electron resulting in an x ray or γ ray in the direction of the electron. The energy $\hbar\omega_X$ of this photon for a scattering angle θ between electron and incoming photon is known as the cut-off energy and given by

$$\hbar\omega_X = 2\hbar\omega_0(1-\cos\theta)\gamma^2, \tag{1}$$

where γ is the Lorentz factor of the electron and $\hbar\omega_0$ is the initial photon energy. For the scattering of laser pulses and electron bunches, the Thomson spectrum is broadened [17–20] and its peak shifted to lower energies compared with the cut-off energy. The divergence of the electron bunch and the normalized vector potential a_0 of the scattering laser in particular can have a large influence on the resulting x-ray spectrum as described by Krämer *et al.* [19], who investigated this effect experimentally. To account for these effects, we introduce a factor Λ which describes the ratio of the peak of the x-ray spectrum and the cut-off energy. The Lorentz factor of the electron beam can be determined by

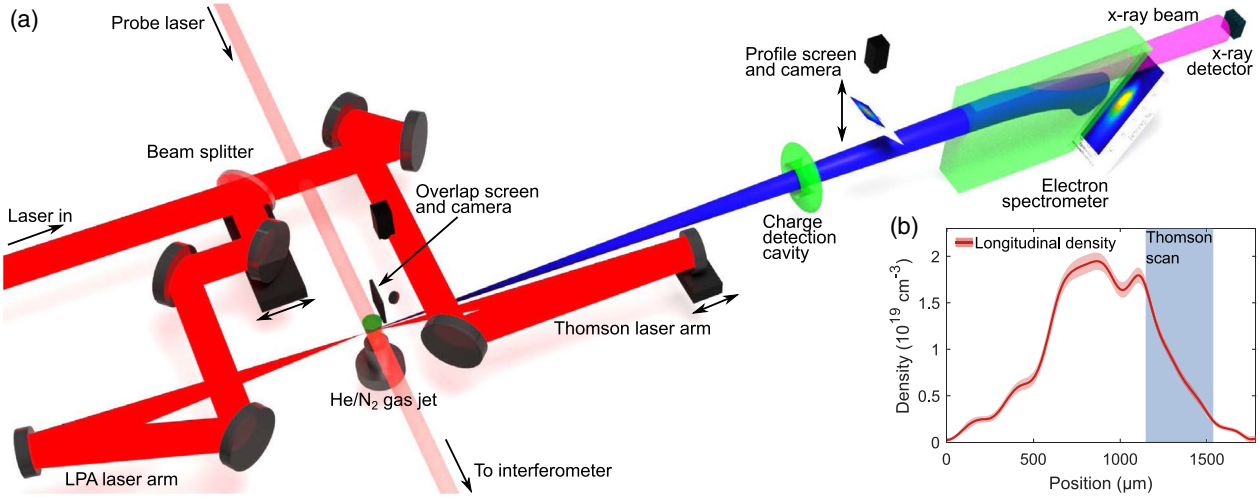

FIG. 1. (a) Schematic of the experimental setup. (b) Mean measured longitudinal plasma density profile with its standard deviation and the region where the Thomson measurement was performed.

measuring the spectrum of the scattered x-ray beam and rearranging Eq. (1) to

$$\gamma = \sqrt{\frac{\hbar\omega_X}{2\Lambda\hbar\omega_0(1-\cos\theta)}}. \tag{2}$$

By overlapping the electron bunch and the Thomson laser at different locations inside plasma it is possible to infer electron-beam properties during acceleration. The information can be transported through the wakefield without significant plasma interaction as the scattered radiation is typically in the hard x-ray range for highly relativistic electrons generated via LPA [21–27].

The experimental setup is schematically depicted in Fig. 1(a). The laser was operated at a repetition rate of 1.4 Hz, and its energy of (190 ± 3) mJ was split using a 5 mm thick MgF beam splitter, resulting in an energy of (125 ± 2) mJ in the LPA laser arm and (65 ± 1) mJ in the Thomson path. The LPA laser pulse was focused with an $f/12$ off-axis parabola to a $1/e^2$ intensity radius of (8.0 ± 0.2) μm. The FWHM pulse duration of the LPA laser was minimized to (26.9 ± 0.2) fs, measured with self-referenced spectral interferometry [28], resulting in a peak vacuum a_0 of 1.18 ± 0.04. However, for optimization of the electron bunches, the pulse was stretched using an acousto-optic dispersive filter [29]. The plasma source was a 1 mm diameter gas jet operated with a gas mix of 99.5% helium and 0.5% nitrogen by weight and a backing pressure of (4.7 ± 0.1) bar. Laser interferometry measurements using a perpendicular probe beam revealed a peak plasma density of $(1.9 \pm 0.1) \times 10^{19}$ cm^{-3} as shown in the density profile in Fig. 1(b). The Thomson laser was focused using a spherical mirror at an incidence angle of 4 degrees resulting in a FWHM spot size of 52 μm by 23 μm. For optimum performance, the scattering laser spot size should be much larger than the electron bunch size which is typically on the order of a few micrometers or less at the used densities [30–32], and its shot-to-shot positional fluctuations should be much smaller than the laser spot. The pulse length after the beam splitter was measured to be (31.1 ± 0.6) fs, leading to a peak vacuum a_0 of 0.31 ± 0.01 in the Thomson laser focus. The Thomson laser crossed the electron beam axis at an offset angle of 8 degrees to prevent backpropagation and damage of upstream laser optics and to allow the x-ray beam to pass.

In order to change the longitudinal focus position of the Thomson laser the spherical mirror was mounted on a linear stage with its axis of movement parallel to the electron beam axis. To resynchronize the electron bunch and the Thomson laser, a delay stage was placed in the LPA laser arm. In the experiment LPA and Thomson laser were inherently synchronized as they were derived from the same laser source. In general, the temporal jitter between the two lasers should be well below the pulse duration of the scattering laser which then determines the longitudinal resolution of the diagnostic. The two laser beams were overlapped in space using a screen which could be driven to a desired overlap plane. The focal plane of the Thomson laser was adjusted to the overlap plane using the linear stage of the spherical mirror. For the temporal alignment of the two laser beams the two generated ionization channels in the gas plume were imaged using interferometry with an independently timed probe beam, similarly to Ref. [26].

Electron and x-ray beam diagnostics were installed downstream of the LPA. The charge of the bunches was measured using a noninvasive cavity-based resonator (DaMon) [33,34], placed 1.1 m from the electron source. The beam profile and pointing stability were measured on a DRZ-type phosphor screen [35,36], driven into the electron beam at a distance of 1.3 m from the gas jet. The electron spectrum was measured using a spectrometer consisting of

a 50 cm long vertically dispersive dipole magnet with a field of 0.14 T and a DRZ screen, supporting a bandwidth of 35 to 250 MeV. This spectrometer did not image the electron source; consequently the measured spectrum appears broadened due to the divergence of the electron beam. The x-ray spectrum was taken using a HEXITEC detector [37,38] which consists of 80×80 CdTe pixels with a size of 250×250 μm^2 and a thickness of 1 mm. To enable single photon counting, the detector was placed 7.8 m from the Thomson interaction point, resulting in a measurement of the on axis x-ray spectrum with an opening angle of ± 1.25 mrad limited by the chip size.

The measured x-ray spectrum is influenced by absorption from 1.7 mm aluminum in the x-ray beamline and the detection cross sections. To extract the source spectrum from the measurements, a full reconstruction of the x-ray transport and detector response was performed in GEANT4 [39–41], and the detection of x-ray beams with a peak energy between 30 keV and 100 keV was simulated in steps of 1 keV. The resulting simulated detector signal was then fitted by a sum of two Gaussian distributions with a separation of 25 keV to account for the escape peak [42] originating from CdTe fluorescence x rays (23–27 keV) leaving the detector [37,38]. The spectral region around the fluorescence peak and events with an energy < 10 keV, which predominantly originate from detector noise, were excluded from the fit. An example of a Gaussian source spectrum with a bandwidth matching that of our measurements, the simulated detector signal according to GEANT4, and the fit are depicted in Fig. 2(a). From this figure, it is evident that the source spectrum and detector signal have similar bandwidth, while the peak of the detector signal is shifted with respect to the source spectrum. The peaks of the fits of the detector signal for all simulations are shown in Fig. 2(b). The simulations highlight that the detector signal overestimates the peak energy of source spectra with a peak energy of < 50 keV due to filtering of low-energy x rays in the aluminum. For source spectra with a peak energy > 55 keV, the detector signal is underestimated due to the lower quantum efficiency of the 1 mm thick CdTe for high-energy x rays. To compensate for these effects, the peaks of measured Thomson spectra are adjusted according to the calibration function shown in Fig. 2(b) to retrieve the spectral peak energy at the source.

The electron beam was generated via self-truncated ionization injection using a weakly relativistic laser [43,44], resulting in spectrally stable and reproducible electron beams, as demonstrated in previous experiments using similar injection methods [45–48]. During the experiment, a FWHM electron-beam pointing stability of 1.4 mrad was measured in the nondispersive axis of the electron spectrometer. It was observed to be equal in both axes in dedicated pointing measurements using the profile screen prior to the main experiments. The profile screen also yielded a beam divergence of (3.9 ± 0.7) mrad horizontally and (7.4 ± 1.6) mrad vertically. Owing to the specific experimental geometry and to ensure the x-ray detector occupancy was low enough to enable single photon counting while also minimizing the background of bremsstrahlung, the charge of the electron beams was kept low by reducing the laser energy to the stated values, limiting the charge to (2.7 ± 1.2) pC. This is a specific limit in our experiment due to the experimental geometry and type of detector. For other shielding geometries or detectors [49–51], higher charges can be measured and would increase the signal further to enhance the accuracy of the measurement. The electron beam energy was stable over the scan of more than 7000 shots to within 1% with a spectral peak of the final electron energy of (61.3 ± 0.5) MeV. The normalized, average spectra of two consecutive sets of 340 shots with and without the Thomson interaction are depicted in Fig. 3 highlighting the excellent spectral stability as well as the noninvasive character of the Thomson interaction.

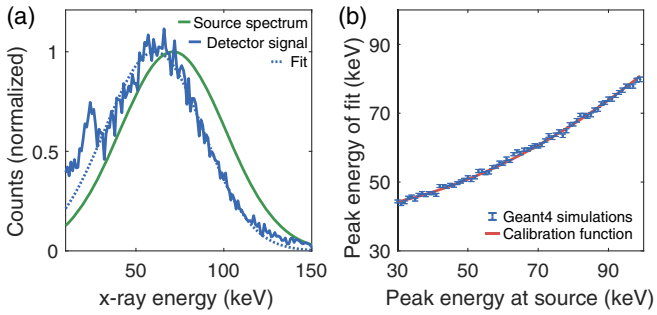

FIG. 2. Simulation of x-ray transport and detection. (a) An x-ray source spectrum (green), the detector signal of this x-ray beam (solid blue), and the double Gaussian fit used to determine the peak of the deposited energy distribution (dotted blue). (b) Peak of the detector signal and 68% confidence intervals from fitting routine as a function of the peak energy of the source spectrum (blue). The calibration function (red) is used for the adjustment of measured data.

Using Thomson scattering, the electron beam energy was then measured at a total of 20 different laser-electron interaction points, enabling a reconstruction of the electron beam energy evolution over a distance of 400 μm in the downramp of the plasma density profile, as shown in Fig. 4. At each overlap position, the signal of 280 shots was integrated on the x-ray detector. The bremsstrahlung background was determined in three dedicated background measurements for which the Thomson laser was blocked. The background-subtracted spectra were then fitted to the sum of two Gaussians as described earlier. Afterward, the peak of the fit to the measurement was adjusted according to the calibration function depicted in Fig. 2(b) to obtain the peak energy of the x-ray spectrum at its source. The peak energy of the Thomson spectrum was then used to calculate the peak electron bunch energy using Eq. (2). The Λ factor was determined experimentally by comparing the energy of

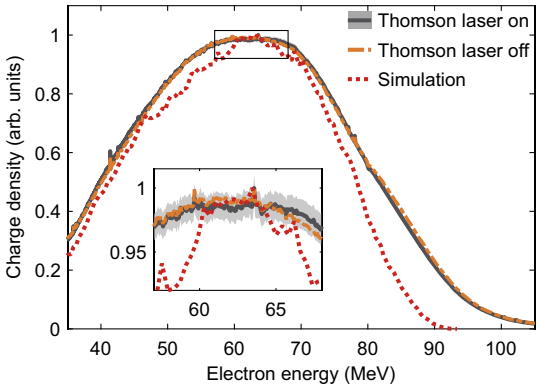

FIG. 3. Normalized electron spectrum of 340 shots with Thomson laser turned on at an overlap position of 1330 μm (gray line), the standard error from individual normalized shots (gray area) and the normalized electron spectrum at the same overlap position without the Thomson laser (orange dashed line). The error band without the Thomson laser is similar to the displayed band with the Thomson laser activated. The same level of agreement between signal and background shots was also observed at overlap positions of 1190 μm and 1560 μm. The region around the peak is shown in more detail in the inset. The spectrum obtained from PIC simulations is depicted as a red dotted line. All lines are normalized individually.

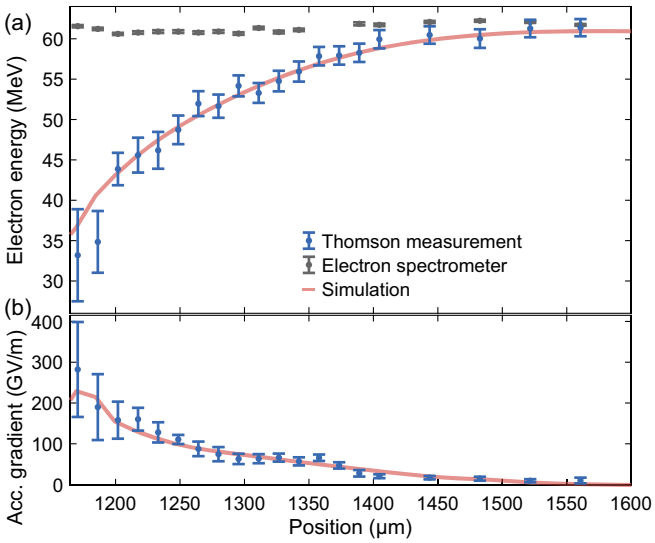

FIG. 4. (a) Electron beam energy measured via Thomson scattering as function of the overlap position (blue). The final electron beam energy at each interaction point is shown as the average peak of Gaussian fits to the single electron spectra with its standard error (gray). The energy evolution obtained from the PIC simulation is shown as a red line, for better comparison again using Gaussian fits. (b). Acceleration gradient as function of the overlap position. The acceleration gradient was calculated using a linear fit of ±3 data points. At the edges only available data points were included. The error bars display the 68% confidence interval.

the electron spectrometer measurement to the Thomson measurement at the last two interaction points, where the measurement suggests constant electron energies and the measured acceleration gradient, likely outside plasma, is negligible. The found value of $\Lambda = 0.89 \pm 0.02$ agrees well with values shown by Krämer *et al.* of approximately 0.90 for using similar electron bunch and laser parameters [19]. In the measurement region, peak electron energies of (34 ± 5) MeV up to (61 ± 1) MeV were detected. The beam energy evolution indicates an acceleration-gradient decrease in the downramp of the plasma from (265 ± 119) GV/m to (9 ± 4) GV/m. The relative error of the acceleration gradient is reduced with more sampling points, reaching as low as 10% in the middle of the scan, as depicted in Fig. 4. These results constitute the first longitudinally resolved *in situ* detection of the on axis accelerating field in a plasma wakefield accelerator, improving on previous integrated results [52–54]. The measurement of the electron energy via Thomson scattering at overlap positions further inside the plasma was not possible, as the energy of the x-ray beam was below the detection threshold of 30 keV owing to absorption in the 1.7 mm aluminum shield in front of the detector. In Fig. 4(a), the evolution of the electron beam energy is compared to the final electron energy measured using the electron spectrometer. As the absolute position of the overlap with respect to the density has an uncertainty of a few hundred μm, the experimental dataset was shifted in the propagation axis to align with the simulation results by minimizing the least squares of the difference of measured data points and the simulated energy evolution (see below). The relative distance between the overlap positions was not affected by this shift and is well defined; the total uncertainty of the scan distance is less than 0.5%. The constant value of the final electron energy simultaneously measured using the spectrometer highlights the noninvasive nature of the demonstrated technique.

Simulations were performed using FBPIC [55,56] to understand the energy gain in the plasma in more detail. In the simulation, laser and plasma parameters similar to those in the experiments were used. The plasma density profile depicted in Fig. 1(b) was imported. For the laser, a pulse duration of 35 fs, a $1/e^2$ intensity radius of 8.0 μm, and a vacuum a_0 of 1.15 were chosen under the assumption of a Gaussian pulse in time and space. The simulation box with a length of 40 μm and a radius of 30 μm was divided in 2000 longitudinal and 128 radial grid points and 36 particles per cell. The laser focus position was scanned in the simulations to match the electron energies of the experiment, and a vacuum focus at 1025 μm resulted in good agreement of the electron energy in the simulation and the spectrometer measurements (cf. Fig. 3). The electron charge in the simulation was 1.8 pC, well within the standard deviation of the experiment. The comparison of the electron-beam-energy evolution and the resulting acceleration gradients of the *in situ* Thomson measurements and the PIC simulation agree well as depicted in Fig. 4.

Thomson measurements could therefore be used to directly study the evolution of the electron bunch in experiments. In combination with control of the longitudinal density, this diagnostic could improve schemes proposed to overcome the dephasing limit in LPA [57–59]. As it is sufficient to only detect the peak of the x-ray spectrum, the technique is compatible with the use of a single-shot x-ray spectrometer, available for a broad range of x-ray and γ-ray energies [49–51]. To improve the signal-to-noise ratio, this method could also be used with traveling-wave Thomson scattering [60] at the cost of spatial resolution while maintaining the noninvasive character of the measurement that requires the use of moderate intensities of the scattering laser [61]. The technique may be extended to diagnose the evolution of other electron beam parameters such as emittance and energy spread [27], and angular distribution [19,62,63] or could be employed in an orthogonal geometry [64] to study the evolution of the longitudinal profile of the electron bunch. Thus, a complete picture of the electron bunch during its acceleration in the wakefield could be obtained to provide the necessary input to optimize the quality of LPA electron beams.

In summary, we have demonstrated a noninvasive measurement of the electron-bunch-energy evolution during its acceleration inside a plasma wakefield via Thomson scattering. Individual beam energy measurements over a 400 μm section of the plasma show an increase of the electron beam energy from (34 ± 5) MeV up to the final energy of (61 ± 1) MeV. This enabled the first longitudinally resolved measurement of the on axis acceleration gradient in a plasma wakefield accelerator and showed a decrease from (265 ± 119) GV/m to (9 ± 4) GV/m in a plasma density down-ramp. These results agree well with simulations, showing the capability to accurately measure the local energy of and accelerating field experienced by the electron beam. Such noninvasive measurements will be crucial to understand the origin of beam-parameter changes, including emittance growth and energy spread in plasma accelerators and subsequently play a key role in improving the quality of electron bunches.

The authors would like to thank M. Dinter, S. Karstensen, S. Kottler, K. Ludwig, F. Marutzky, A. Rahali, V. Rybnikov, and A. Schleiermacher for their engineering and technical support and the Central Laser Facility from the Science and Technology Facilities Council, UK, for providing a HEXITEC detector. The authors acknowledge funding from Helmholtz ARD, Helmholtz ATHENA, the DESY Strategy Fund, and the BMBF InnovationPool through project PLASMED X. This work was supported by the Maxwell computational resources at DESY.

*simon.bohlen@desy.de

[1] T. Tajima and J. M. Dawson, Laser Electron Accelerator, Phys. Rev. Lett. **43**, 267 (1979).

[2] S. P. D. Mangles, C. D. Murphy, Z. Najmudin, A. G. R. Thomas, J. L. Collier, A. E. Dangor, E. J. Divall, P. S. Foster, J. G. Gallacher, C. J. Hooker, D. A. Jaroszynski, A. J. Langley, W. B. Mori, P. A. Norreys, F. S. Tsung, R. Viskup, B. R. Walton, and K. Krushelnick, Monoenergetic beams of relativistic electrons from intense laser–plasma interactions, Nature (London) **431**, 535 (2004).

[3] C. G. R. Geddes, C. Toth, J. van Tilborg, E. Esarey, C. B. Schroeder, D. Bruhwiler, C. Nieter, J. Cary, and W. P. Leemans, High-quality electron beams from a laser wakefield accelerator using plasma-channel guiding, Nature (London) **431**, 538 (2004).

[4] J. Faure, Y. Glinec, A. Pukhov, S. Kiselev, S. Gordienko, E. Lefebvre, J.-P. Rousseau, F. Burgy, and V. Malka, A laser–plasma accelerator producing monoenergetic electron beams, Nature (London) **431**, 541 (2004).

[5] H. T. Kim, K. H. Pae, H. J. Cha, I. J. Kim, T. J. Yu, J. H. Sung, S. K. Lee, T. M. Jeong, and J. Lee, Enhancement of Electron Energy to the Multi-GeV Regime by a Dual-Stage Laser-Wakefield Accelerator Pumped by Petawatt Laser Pulses, Phys. Rev. Lett. **111**, 165002 (2013).

[6] X. Wang *et al.*, Quasi-monoenergetic laser-plasma acceleration of electrons to 2 GeV, Nat. Commun. **4**, 1988 (2013).

[7] W. P. Leemans, A. J. Gonsalves, H.-S. Mao, K. Nakamura, C. Benedetti, C. B. Schroeder, C. Tóth, J. Daniels, D. E. Mittelberger, S. S. Bulanov, J.-L. Vay, C. G. R. Geddes, and E. Esarey, Multi-GeV Electron Beams from Capillary-Discharge-Guided Subpetawatt Laser Pulses in the Self-Trapping Regime, Phys. Rev. Lett. **113**, 245002 (2014).

[8] A. J. Gonsalves *et al.*, Petawatt Laser Guiding and Electron Beam Acceleration to 8 GeV in a Laser-Heated Capillary Discharge Waveguide, Phys. Rev. Lett. **122**, 084801 (2019).

[9] W. Wang *et al.*, Free-electron lasing at 27 nanometres based on a laser wakefield accelerator, Nature (London) **595**, 516 (2021).

[10] M. C. Downer, R. Zgadzaj, A. Debus, U. Schramm, and M. C. Kaluza, Diagnostics for plasma-based electron accelerators, Rev. Mod. Phys. **90**, 035002 (2018).

[11] Y. Ma, D. Seipt, S. J. D. Dann, M. J. V. Streeter, C. A. J. Palmer, L. Willingale, and A. G. R. Thomas, Angular streaking of betatron X-rays in a transverse density gradient laser-wakefield accelerator, Phys. Plasmas **25**, 113105 (2018).

[12] J. Faure, C. Rechatin, A. Norlin, A. Lifschitz, Y. Glinec, and V. Malka, Controlled injection and acceleration of electrons in plasma wakefields by colliding laser pulses, Nature (London) **444**, 737 (2006).

[13] K. K. Swanson, H. E. Tsai, S. K. Barber, R. Lehe, H. S. Mao, S. Steinke, J. van Tilborg, K. Nakamura, C. G. R. Geddes, C. B. Schroeder, E. Esarey, and W. P. Leemans, Control of tunable, monoenergetic laser-plasma-accelerated electron beams using a shock-induced density downramp injector, Phys. Rev. Accel. Beams **20**, 051301 (2017).

[14] D. E. Cardenas, S. Chou, E. Wallin, J. Xu, L. Hofmann, A. Buck, K. Schmid, D. E. Rivas, B. Shen, A. Gonoskov, M. Marklund, and L. Veisz, Electron bunch evolution in laser-wakefield acceleration, Phys. Rev. Accel. Beams **23**, 112803 (2020).

[15] K. Poder, J. C. Wood, N. C. Lopes, J. M. Cole, S. Alatabi, P. S. Foster, C. Kamperidis, O. Kononenko, C. A. J. Palmer, D. Rusby, A. Sahai, G. Sarri, D. R. Symes, J. R. Warwick, S. P. D. Mangles, and Z. Najmudin, Multi-GeV electron acceleration in wakefields strongly driven by oversized laser spots (to be published).

[16] J. J. Thomson, *Conductivity of Electricity through Gases* (Cambridge University Press, Cambridge, England, 1906).

[17] W. J. Brown, S. G. Anderson, C. P. J. Barty, S. M. Betts, R. Booth, J. K. Crane, R. R. Cross, D. N. Fittinghoff, D. J. Gibson, F. V. Hartemann, E. P. Hartouni, J. Kuba, G. P. Le Sage, D. R. Slaughter, A. M. Tremaine, A. J. Wootton, P. T. Springer, and J. B. Rosenzweig, Experimental characterization of an ultrafast Thomson scattering x-ray source with three-dimensional time and frequency-domain analysis, Phys. Rev. ST Accel. Beams **7**, 060702 (2004).

[18] S. G. Rykovanov, C. G. R. Geddes, J.-L. Vay, C. B. Schroeder, E. Esarey, and W. P. Leemans, Quasi-monoenergetic femtosecond photon sources from Thomson Scattering using laser plasma accelerators and plasma channels, J. Phys. B **47**, 234013 (2014).

[19] J. M. Krämer, A. Jochmann, M. Budde, M. Bussmann, J. P. Couperus, T. E. Cowan, A. Debus, A. Köhler, M. Kuntzsch, A. Laso García, U. Lehnert, P. Michel, R. Pausch, O. Zarini, U. Schramm, and A. Irman, Making spectral shape measurements in inverse Compton scattering a tool for advanced diagnostic applications, Sci. Rep. **8**, 1398 (2018).

[20] T. Brümmer, A. Debus, R. Pausch, J. Osterhoff, and F. Grüner, Design study for a compact laser-driven source for medical x-ray fluorescence imaging, Phys. Rev. Accel. Beams **23**, 031601 (2020).

[21] H. Schwoerer, B. Liesfeld, H. P. Schlenvoigt, K. U. Amthor, and R. Sauerbrey, Thomson-Backscattered X Rays From Laser-Accelerated Electrons, Phys. Rev. Lett. **96**, 014802 (2006), 10.1103/PhysRevLett.96.014802.

[22] K. Ta Phuoc, S. Corde, C. Thaury, V. Malka, A. Tafzi, J. P. Goddet, R. C. Shah, S. Sebban, and A. Rousse, All-optical Compton gamma-ray source, Nat. Photonics **6**, 308 (2012).

[23] S. Chen, N. D. Powers, I. Ghebregziabher, C. M. Maharjan, C. Liu, G. Golovin, S. Banerjee, J. Zhang, N. Cunningham, A. Moorti, S. Clarke, S. Pozzi, and D. P. Umstadter, MeV-Energy X Rays from Inverse Compton Scattering with Laser-Wakefield Accelerated Electrons, Phys. Rev. Lett. **110**, 155003 (2013).

[24] N. D. Powers, I. Ghebregziabher, G. Golovin, C. Liu, S. Chen, S. Banerjee, J. Zhang, and D. P. Umstadter, Quasi-monoenergetic and tunable X-rays from a laser-driven Compton light source, Nat. Photonics **8**, 28 (2014).

[25] G. Sarri, D. J. Corvan, W. Schumaker, J. M. Cole, A. Di Piazza, H. Ahmed, C. Harvey, C. H. Keitel, K. Krushelnick, S. P. D. Mangles, Z. Najmudin, D. Symes, A. G. R. Thomas, M. Yeung, Z. Zhao, and M. Zepf, Ultrahigh Brilliance Multi-MeV γ-Ray Beams from Nonlinear Relativistic Thomson Scattering, Phys. Rev. Lett. **113**, 224801 (2014).

[26] K. Khrennikov, J. Wenz, A. Buck, J. Xu, M. Heigoldt, L. Veisz, and S. Karsch, Tunable All-Optical Quasimonochromatic Thomson X-Ray Source in the Nonlinear Regime, Phys. Rev. Lett. **114**, 195003 (2015).

[27] G. Golovin, S. Banerjee, C. Liu, S. Chen, J. Zhang, B. Zhao, P. Zhang, M. Veale, M. Wilson, P. Seller, and D. Umstadter, Intrinsic beam emittance of laser-accelerated electrons measured by x-ray spectroscopic imaging, Sci. Rep. **6**, 24622 (2016).

[28] T. Oksenhendler, S. Coudreau, N. Forget, V. Crozatier, S. Grabielle, R. Herzog, O. Gobert, and D. Kaplan, Self-referenced spectral interferometry, Appl. Phys. B **99**, 7 (2010).

[29] P. Tournois, Acousto-optic programmable dispersive filter for adaptive compensation of group delay time dispersion in laser systems, Opt. Commun. **140**, 245 (1997).

[30] S. Kneip *et al.*, Bright spatially coherent synchrotron X-rays from a table-top source, Nat. Phys. **6**, 980 (2010).

[31] G. R. Plateau, C. G. R. Geddes, D. B. Thorn, M. Chen, C. Benedetti, E. Esarey, A. J. Gonsalves, N. H. Matlis, K. Nakamura, C. B. Schroeder, S. Shiraishi, T. Sokollik, J. vanTilborg, C. Toth, S. Trotsenko, T. S. Kim, M. Battaglia, T. Stöhlker, and W. P. Leemans, Low-Emittance Electron Bunches from a Laser-Plasma Accelerator Measured using Single-Shot X-Ray Spectroscopy, Phys. Rev. Lett. **109**, 064802 (2012).

[32] M. Schnell, A. Sävert, B. Landgraf, M. Reuter, M. Nicolai, O. Jäckel, C. Peth, T. Thiele, O. Jansen, A. Pukhov, O. Willi, M. C. Kaluza, and C. Spielmann, Deducing the Electron-Beam Diameter in a Laser-Plasma Accelerator Using X-Ray Betatron Radiation, Phys. Rev. Lett. **108**, 075001 (2012).

[33] D. Lipka, W. Kleen, J. Lund-Nielsen, D. Nölle, S. Vilcins, and V. Vogel, Dark Current Monitor for the European XFEL, in *Proceedings of the DIPAC2011* (JACow, Hamburg, Germany, 2011), pp. 572–574.

[34] D. Lipka, J. Lund-Nielsen, and M. Seebach, Resonator for Charge Measurement at REGEA, in *Proceedings of the IBIC2013* (JACow, Oxford, UK, 2013), pp. 872–875.

[35] T. Kurz, J. P. Couperus, J. M. Krämer, H. Ding, S. Kuschel, A. Köhler, O. Zarini, D. Hollatz, D. Schinkel, R. D'Arcy, J.-P. Schwinkendorf, J. Osterhoff, A. Irman, U. Schramm, and S. Karsch, Calibration and cross-laboratory implementation of scintillating screens for electron bunch charge determination, Rev. Sci. Instrum. **89**, 093303 (2018).

[36] J.-P. Schwinkendorf, S. Bohlen, J. Couperus Cabadağ, H. Ding, A. Irman, S. Karsch, A. Köhler, J. Krämer, T. Kurz, S. Kuschel, J. Osterhoff, L. Schaper, D. Schinkel, U. Schramm, O. Zarini, and R. D'Arcy, Charge calibration of DRZ scintillation phosphor screens, J. Instrum. **14**, P09025 (2019).

[37] P. Seller, S. Bell, R. J. Cernik, C. Christodoulou, C. K. Egan, J. A. Gaskin, S. Jacques, S. Pani, B. D. Ramsey, C. Reid, P. J. Sellin, J. W. Scuffham, R. D. Speller, M. D. Wilson, and M. C. Veale, Pixellated Cd(Zn)Te high-energy X-ray instrument, J. Instrum. **6**, C12009 (2011).

[38] M. C. Veale, P. Seller, M. Wilson, and E. Liotti, HEXITEC: A High-Energy X-ray Spectroscopic Imaging Detector for Synchrotron Applications, Synchrotron Radiat. News **31**, 28 (2018).

[39] S. Agostinelli *et al.*, Geant4—a simulation toolkit, Nucl. Instrum. Methods Phys. Res., Sect. A **506**, 250 (2003).

[40] J. Allison *et al.*, Geant4 developments and applications, IEEE Trans. Nucl. Sci. **53**, 270 (2006).

[41] J. Allison *et al.*, Recent developments in Geant4, Nucl. Instrum. Methods Phys. Res., Sect. A **835**, 186 (2016).
[42] R. H. Redus, J. A. Pantazis, T. J. Pantazis, A. C. Huber, and B. J. Cross, Characterization of CdTe Detectors for Quantitative X-ray Spectroscopy, IEEE Trans. Nucl. Sci. **56**, 2524 (2009).
[43] M. Zeng, M. Chen, Z.-M. Sheng, W. B. Mori, and J. Zhang, Self-truncated ionization injection and consequent monoenergetic electron bunches in laser wakefield acceleration, Phys. Plasmas **21**, 030701 (2014).
[44] C. Kamperidis, V. Dimitriou, S. P. Mangles, A. E. Dangor, and Z. Najmudin, Low energy spread electron beams from ionization injection in a weakly relativistic laser wakefield accelerator, Plasma Phys. Controlled Fusion **56**, 084007 (2014).
[45] M. Mirzaie, S. Li, M. Zeng, N. A. M. Hafz, M. Chen, G. Y. Li, Q. J. Zhu, H. Liao, T. Sokollik, F. Liu, Y. Y. Ma, L. Chen, Z. M. Sheng, and J. Zhang, Demonstration of self-truncated ionization injection for GeV electron beams, Sci. Rep. **5**, 14659 (2015).
[46] J. P. Couperus, R. Pausch, A. Köhler, O. Zarini, J. M. Krämer, M. Garten, A. Huebl, R. Gebhardt, U. Helbig, S. Bock, K. Zeil, A. Debus, M. Bussmann, U. Schramm, and A. Irman, Demonstration of a beam loaded nanocoulomb-class laser wakefield accelerator, Nat. Commun. **8**, 487 (2017).
[47] A. Irman, J. P. Couperus, A. Debus, A. Köhler, J. M. Krämer, R. Pausch, O. Zarini, and U. Schramm, Improved performance of laser wakefield acceleration by tailored self-truncated ionization injection, Plasma Phys. Controlled Fusion **60**, 044015 (2018).
[48] S. Bohlen, J. C. Wood, T. Brümmer, F. Grüner, C. A. Lindstrøm, M. Meisel, T. Staufer, R. D'Arcy, K. Põder, and J. Osterhoff, Stability of ionization-injection-based laser-plasma accelerators, Phys. Rev. Accel. Beams **25**, 031301 (2022).
[49] D. J. Corvan, G. Sarri, and M. Zepf, Design of a compact spectrometer for high-flux MeV gamma-ray beams, Rev. Sci. Instrum. **85**, 065119 (2014).
[50] K. T. Behm *et al.*, A spectrometer for ultrashort gamma-ray pulses with photon energies greater than 10 MeV, Rev. Sci. Instrum. **89**, 113303 (2018).
[51] A. Hannasch, A. L. Garcia, M. LaBerge, R. Zgadzaj, A. Köhler, J. P. C. Cabadağ, O. Zarini, T. Kurz, A. Ferrari, M. Molodtsova, L. Naumann, T. E. Cowan, U. Schramm, A. Irman, and M. C. Downer, Compact spectroscopy of keV to MeV X-rays from a laser wakefield accelerator, Sci. Rep. **11**, 14368 (2021).
[52] C. E. Clayton, E. Adli, J. Allen, W. An, C. I. Clarke, S. Corde, J. Frederico, S. Gessner, S. Z. Green, M. J. Hogan, C. Joshi, M. Litos, W. Lu, K. A. Marsh, W. B. Mori, N. Vafaei-Najafabadi, X. Xu, and V. Yakimenko, Self-mapping the longitudinal field structure of a nonlinear plasma accelerator cavity, Nat. Commun. **7**, 12483 (2016).
[53] C. J. Zhang, J. F. Hua, Y. Wan, C.-H. Pai, B. Guo, J. Zhang, Y. Ma, F. Li, Y. P. Wu, H.-H. Chu, Y. Q. Gu, X. L. Xu, W. B. Mori, C. Joshi, J. Wang, and W. Lu, Femtosecond Probing of Plasma Wakefields and Observation of the Plasma Wake Reversal Using a Relativistic Electron Bunch, Phys. Rev. Lett. **119**, 064801 (2017).
[54] S. Schröder *et al.*, High-resolution sampling of beam-driven plasma wakefields, Nat. Commun. **12**, 371 (2021).
[55] R. Lehe, M. Kirchen, I. A. Andriyash, B. B. Godfrey, and J. L. Vay, A spectral, quasi-cylindrical and dispersion-free Particle-In-Cell algorithm, Comput. Phys. Commun. **203**, 66 (2016).
[56] S. Jalas, I. Dornmair, R. Lehe, H. Vincenti, J. L. Vay, M. Kirchen, and A. R. Maier, Accurate modeling of plasma acceleration with arbitrary order pseudo-spectral particle-in-cell methods, Phys. Plasmas **24**, 033115 (2017).
[57] P. Sprangle, B. Hafizi, J. R. Peñano, R. F. Hubbard, A. Ting, C. I. Moore, D. E. Gordon, A. Zigler, D. Kaganovich, and T. M. Antonsen, Wakefield generation and GeV acceleration in tapered plasma channels, Phys. Rev. E **63**, 056405 (2001).
[58] E. Guillaume, A. Döpp, C. Thaury, K. Ta Phuoc, A. Lifschitz, G. Grittani, J. P. Goddet, A. Tafzi, S. W. Chou, L. Veisz, and V. Malka, Electron Rephasing in a Laser-Wakefield Accelerator, Phys. Rev. Lett. **115**, 155002 (2015).
[59] J. D. Sadler, C. Arran, H. Li, and K. A. Flippo, Overcoming the dephasing limit in multiple-pulse laser wakefield acceleration, Phys. Rev. Accel. Beams **23**, 021303 (2020).
[60] Q. Chen, V. Horný, R. Syed, and D. Umstadter, Traveling-wave Thomson scattering for electron-beam spectroscopy, Phys. Rev. Accel. Beams **24**, 032901 (2021).
[61] M. J. V. Streeter and Z. Najmudin, Compton recoil effects in staging of laser wakefield accelerators, Phys. Rev. Accel. Beams **23**, 071602 (2020).
[62] K. Chouffani, F. Harmon, D. Wells, J. Jones, and G. Lancaster, Determination of electron beam parameters by means of laser-Compton scattering, Phys. Rev. ST Accel. Beams **9**, 050701 (2006).
[63] A. Jochmann, A. Irman, M. Bussmann, J. P. Couperus, T. E. Cowan, A. D. Debus, M. Kuntzsch, K. W. D. Ledingham, U. Lehnert, R. Sauerbrey, H. P. Schlenvoigt, D. Seipt, T. Stöhlker, D. B. Thorn, S. Trotsenko, A. Wagner, and U. Schramm, High Resolution Energy-Angle Correlation Measurement of Hard X Rays from Laser-Thomson Backscattering, Phys. Rev. Lett. **111**, 114803 (2013).
[64] W. P. Leemans, R. W. Schoenlein, P. Volfbeyn, A. H. Chin, T. E. Glover, P. Balling, M. Zolotorev, K. J. Kim, S. Chattopadhyay, and C. V. Shank, X-Ray Based Subpicosecond Electron Bunch Characterization Using 90° Thomson Scattering, Phys. Rev. Lett. **77**, 4182 (1996).